# Synthesis and Characterization of $MoO_3$ Thin Films and Powders from a Molybdenum Chloromethoxide

Mauro Epifani,*,† Patrizia Imperatori,‡ Luciana Mirenghi,§ Monica Schioppa,§ and Pietro Siciliano†

*Istituto per la Microelettronica ed i Microsistemi, Consiglio Nazionale delle Ricerche, CNR-IMM, sezione di Lecce, 73100 Lecce, Istituto di Struttura della Materia, Consiglio Nazionale delle Ricerche CNR-ISM, 00016 Monterotondo (Roma), and ENEA C.R. Brindisi, UTS MAT, 72100 Brindisi, Italy*

*Received June 24, 2004. Revised Manuscript Received September 2, 2004*

A molybdenum chloromethoxide was prepared by reaction of $MoCl_5$ with methanol. By water addition, a sol was obtained that was stable on a month time scale. The sols were characterized by UV−vis and Raman spectroscopy, showing that upon water addition hydrolysis takes place but without extensive condensation, explaining the sol stability. The sol was modified by addition of cetyltrimethylammonium bromide to get deposition of thin films onto silicon substrates. Very uniform, polycrystalline α-$MoO_3$ thin films on silicon or polycrystalline powders could be obtained after heat treatment at 350 °C of the as-deposited film and the evaporated sol, respectively. Fourier transform infrared and X-ray photoelectron spectroscopy studies on the films and powders have shown that, while the films are extensively polymerized after the deposition and chlorine free, the powders evolve with the heating temperature toward the final structure by a stepwise process in which the Mo(IV) and Mo(V) states are progressively oxidized to the final Mo(VI) state. The powders heated at at least 250 °C are chlorine free. X-ray diffraction patterns measured on thin films and powders show that the films are amorphous up to 250 °C, while powders begin to crystallize as α-$MoO_3$ at such a temperature. These results are supported by thermal analysis on powders. Scanning electron microscopy observations show that the film morphology is initially very smooth while after heating at 500 °C it is constituted by flat micrometric platelets. The powders heated at 500 °C show a lamellar structure.

## Introduction

α-Molybdenum trioxide ($MoO_3$) has a peculiar layered structure composed of distorted $MoO_6$ octahedra,[1] and is of technological interest in such fields as lithium batteries,[2] electrochromic windows,[3] catalysis,[4] and gas sensors.[5] The processing of $MoO_3$ has been recently proposed through soft-chemical routes,[6] with the advantage of the low processing temperatures and the consequent possibility of obtaining amorphous or unusual phases. Among such techniques, the sol−gel process has been employed for preparing $MoO_3$ thin films, gels, and powders, starting from precursors ranging from the oxychlorides[7] and alkoxides[8] to acetylacetonates.[9] In this context, it seemed of particular interest to explore the use of $MoCl_5$ as a precursor to $MoO_3$, since it shows a number of features that could make it an interesting alternative: its low cost makes it preferable to alkoxides, and it has, if compared to $MoOCl_3$, which contains a Mo=O group in its structure, a larger number of hydrolizable bonds and, then, a potentially higher functionality for inorganic polymerization. This property is particularly important in the preparation of uniform thin films, but it is necessary to hinder the formation of Mo=O bonds in the sol since they prevent the formation of monolithic gels.[7b,8b] Dong and Dunn used chemical complexation of molybdenum alkoxides for solving this problem. We decided not to use any complexing additive in the processing of $MoCl_5$ and then to check experimentally whether the initial lack of Mo=O bonds in $MoCl_5$ had been preserved in

* To whom correspondence should be addressed. E-mail: mauro.epifani@imm.cnr.it.
† CNR-IMM.
‡ CNR-ISM.
§ UTS MAT.

(1) (a) McCarron, E. M., III; Thomas, D. M.; Calabrese, J. C. *Inorg. Chem.* **1987**, *26*, 370. (b) Rao, C. N. R.; Raveau, B. *Transition Metal Oxides—Structure, Properties and Synthesis of Ceramic Oxides*, 2nd ed.; Wiley-VCH: New York, 1998; Chapter 7, Part 1.

(2) Ferreira, F. F.; Souza Cruza, T. G.; Fantini M. C. A.; Tabacniks, M. H.; de Castro S. C.; Morais, J.; de Siervo, A.; Landers, R.; Gorenstein, A. *Solid State Ionics* **2000**, *136−137*, 357.

(3) Ivanova, T.; Gesheva, K. A.; Ganchev, M.; Tzvetkova, E. *J. Mater. Sci.: Mater. Electron.* **2003**, *14*, 755.

(4) Reddy, K. R.; Ramesh, K.; Seela, K. K.; Rao, V. V.; Chary, K. V. R. *Catal. Commun.* **2003**, *4*, 112.

(5) Comini, E.; Faglia, G.; Sberveglieri, G.; Cantalini, C.; Passacantando, M.; Santucci, S.; Li, Y.; Wlodarski, W.; Qu, W. *Sens. Actuators, B* **2000**, *68*, 168.

(6) (a) Gerand, B.; Seguin, L. *Solid State Ionics* **1996**, *84*, 199. (b) Juarez Ramirez, I.; Martinez De La Cruz, A. *Mater. Lett.* **2003**, *57*, 1034.

(7) (a) Mendez-Vivar, J.; Campero, A.; Livage, J.; Sanchez, C. *J. Non-Cryst. Solids* **1990**, *121*, 26. (b) Yanovskaya, M. I.; Obvintseva, I. E.; Kessler, V. G.; Galyamov, B. Sh.; Kucheiko, S. I.; Shifrina, R. R.; Turova, N. Ya. *J. Non-Cryst. Solids* **1990**, *124*, 155. (c) Mendez-Vivar, J.; Lopez, T.; Campero, A.; Livage, J.; Sanchez, C. *Langmuir* **1991**, *7*, 704.

(8) (a) Hollinghead, J. A.; Tyszkiewicz, M. T.; McCarley, R. E. *Chem. Mater.* **1993**, *5*, 1600. (b) Dong, W.; Dunn, B. *J. Mater. Chem.* **1998**, *8*, 665.

(9) (a) Mallikarjuna, N. N.; Venkataraman, A. *J. Therm. Anal. Calorim.* **2002**, *68*, 901. (b) Jiebing, S.; Rui, X.; Shimin, W.; Wufeng, T.; Hua, T.; Jing, S. *J. Sol-Gel Sci. Technol*. **2003**, *27*, 315.

10.1021/cm048997i CCC: $27.50 © 2004 American Chemical Society
Published on Web 11/09/2004

the sol stage. It will be shown that this actually occurred and that uniform thin films can indeed be prepared. For comparison, powders were also prepared. The structural and chemical evolution of the $MoO_3$ films and powders was studied by Raman spectroscopy, Fourier transform infrared (FTIR) spectroscopy, X-ray photoelectron spectroscopy (XPS), X-ray diffraction (XRD), and thermal analysis techniques as a function of the heating temperature. The results show that thin films and powders evolve in a markedly different way during the heat treatment. Moreover, due to our interest in the deposition of thin films onto silicon substrates for the processing of integrated devices, and since it is difficult to obtain adherent and uniform films on such substrates when working with inorganic precursors, this study also introduces cethyltrimethylammonium bromide (CTAB) as a general additive for overcoming such problems.

## Experimental Section

$MoCl_5$ (Acros Organics), methanol, and CTAB (Aldrich) were used as received. Silicon substrates (⟨100⟩ orientation) with a 5000 Å $SiO_2$ overlayer were provided by ST Microelectronics. For preparing $MoO_3$ sols, in a glovebox (Braun, LabStar) with $[H_2O] < 1$ ppm, 10 mL of MeOH was slowly added to 1 g of $MoCl_5$. A green solution was obtained, with evolution of HCl and heat. After the solution was cooled, it was taken out of the glovebox, and water was added dropwise. Different $H_2O$:Mo molar ratios, denoted hereafter as $r$, were employed, ranging from 0 to 4. Films and powders for the various characterizations were prepared from the sols with a $H_2O$:Mo molar ratio of 4, since it provided the most uniform films and minimized the amount of hexagonal $MoO_3$, as seen in the XRD patterns shown below. After 24 h had passed since water addition, 100 mg of CTAB was poured into the sol. Thin films were prepared by spin-coating the obtained sols at 2000 rpm onto the silicon substrates, precleaned for 2 min in boiling 2-propanol. The films were dried for 5 min at 70 °C in air and then heat-treated for 1 h at temperatures ranging from 150 to 500 °C in an air atmosphere, with a heating rate of 250 °C/h. The films were very uniform and crackless after the various heat treatments, becoming white-opaque after the heat treatment at 500 °C. The thickness of a film heat-treated at 350 °C was about 110 nm, as measured with a profilometer (Tencor Instruments, Alpha-Step IQ). Powders were prepared from the sols by evaporating the solvent in a rotary evaporator, at a pressure decreased from 100 to 40 mbar in about 30 min and with the bath temperature raised from room temperature to 70 °C in about 1 h. The evaporation product was heat-treated at various temperatures similarly to the thin films.

UV−vis optical absorption spectra on the sols were obtained on a Perkin-Elmer model Lambda 19 spectrophotometer, after further dilution of the sols in methanol.

The green line of a Jobin Yvon T64000 Raman spectrometer with a Coherent Innova 300 Ar laser and a bidimensional CCD detector cooled with liquid nitrogen was used for Raman analysis of the sols. The sol with $r = 0$ was prepared and tightly sealed in a glass vial in the glovebox to avoid any contamination with moisture.

FTIR spectra were acquired with a Nicolet SX800 spectrometer in transmission mode on the thin films deposited onto the silicon substrates, subtracting the contribution of the uncoated substrate. FTIR spectra on the powders were measured on pellets prepared by mixing the powders with KBr with a sample:KBr volume ratio of about 1:50.

XPS surface analyses have been performed with an ESCALAB 210 spectrometer by VG Scientific. The X-ray source employed was a nonmonochromatized Mg $K\alpha_{1,2}$ twin anode working at 300 W. The experimental spectra were acquired in standard conditions and "large area mode" for the input analyzer lens setup. The UHV conditions of the main analyzer chamber and the constant pass energy of the hemispherical analyzer ensured the best conditions for no surface contamination during the acquisition time and a constant energy resolution at all the kinetic energies for the peaks. The energy position of the peaks was assessed by a calibration routine, using the Ag $3d_{5/2}$ line at 368.26 eV acquired on a standard silver film used as a reference sample. The powders were fixed at the sample holder with a biadhesive film, giving them a certain amount of surface charging on all the peak positions of the main narrow scan spectra acquired: Mo 3d, O 1s, C 1s, Cl 2p. They were all properly corrected with respect to the adventitious C 1s present on the surface with respect to the tabulated and literature value of 284.6 eV. Optimized input parameters and background subtraction procedures (Shirley for the 70 °C sample and linear for the 250 and 500 °C samples) were employed to obtain the best fits and low $\chi^2$ values.

Simultaneous thermogravimetry−differential thermal analysis (TG−DTA) was employed to investigate the thermal evolution of the $MoO_3$ precursor, in nonisothermal conditions. The measurements were carried out using a NETZSCH STA 429 simultaneous thermal analyzer equipped with a NiCr/CuNi thermocouple. A sample mass of about 10 mg was heated to 500 °C into an open aluminum crucible at a rate of 3 °C/min, in a static air atmosphere.

XRD measurements on the thin films were performed on a Seifert 3003 TT diffractometer equipped with a thin film attachment consisting of long Soller slits and a flat graphite monochromator. The diffraction patterns were recorded using Cu Kα radiation ($\lambda = 1.5418$ Å). Data were collected in a grazing incidence geometry at an incident angle of 1°. Values of $2\theta$ were in the range 1.5−80°, the step size was 0.02°, and the counting time was 8 s/step. The crystallite size was estimated from the full width at half-maximum (fwhm) of the ($0k0$) reflections, after correction for instrumental peak broadening, applying the Warren−Averbach method[10] on multiple order reflections. XRD measurements on the powders were carried out on a Philips PW1880 diffractometer.

The morphology of the thin films and the powders was observed with a JEOL JSM6500F FEG scanning electron microscope.

## Results and Discussion

**A. Sol Preparation**. When methanol was added to $MoCl_5$, an emerald green solution was obtained, due to the formation of the dimer $[MoCl_3(OR)_2]_2$.[11] The solution became green-brown upon water addition, and remained clear. The sols with $r = 4$ were stable for at least 6 months, after which a deep blue precipitate formed on the walls and the bottom of the container. When using 1-butanol instead of methanol, the sol stability was much decreased, probably because of enhanced hydrolysis consequent to alcohol esterification with HCl present as a byproduct.[11] The chloromethoxide is very prone to hydrolysis since it is just necessary to leave a drop shortly exposed to the atmosphere for seeing the color change from green to green-brown. The UV−vis optical absorption spectra measured on the sols prepared with different $r$ values are shown in Figure 1. They display basically the same structure, with an intense band at about 440 nm and a weaker band at about 720 nm, due to d−d electronic transitions in the Mo(V) complex.[12] Changing the $r$ value from 0 to 1 initially results in an evident shape change of the bands and of the intensity of absorption. This result reflects a change of symmetry

(10) Warren, B. E.; Averback, B. L. *J. Appl. Phys.* **1950**, *21*, 595.
(11) (a) Bradley, D. C.; Multani, R. K.; Wardlaw, W. *J. Chem. Soc.* **1958**, 4647. (b) Bradley, D. C.; Mehrotra, R. C.; Gaur, D. P. *Metal Alkoxides*; Academic Press: London, 1978; p 18.
(12) McClung, D. A.; Dalton, L. R.; Brubaker, C. H. *Inorg. Chem.* **1966**, *5*, 1985.

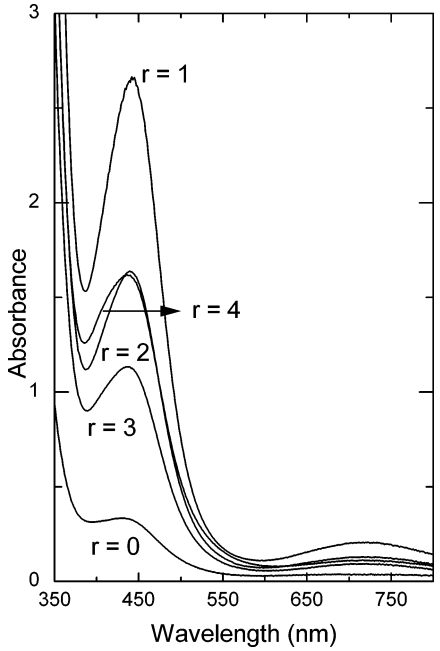


**Figure 1.** Optical absorption spectra measured on sols prepared with the indicated values of the hydrolysis ratio.

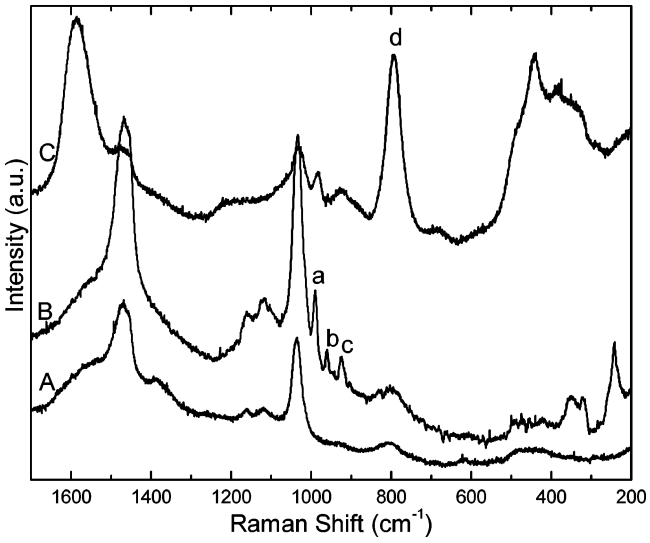


**Figure 2.** Raman spectra measured on sols with $r = 0$ (curve B) and $r = 4$ (curve C). The spectrum of methanol is shown as curve A as a reference. The peaks indicated with a−d are described in the text.

of the complex and, then, a different environment of Mo ions due to the substitution of chloro and alkoxo ligands with hydroxo ligands from hydrolysis and, eventually, to the formation of Mo−O−Mo bridges from condensation reactions. Nevertheless, the sol stability indicates that condensation occurs very slowly; thus, hydrolysis should be the prevalent reaction in the early stages of sol formation. For $r$ values higher than 1, the spectral modifications are less evident but still indicate further changes in the Mo coordination. Further insight into the sol structure could be obtained by Raman spectroscopy, whose results are shown in Figure 2, where curve A refers to methanol and is shown as a reference while curve B refers to a sol with $r = 0$ and curve C to a sol with $r = 4$. To the best of our knowledge, Raman spectra have not been reported for such a system; thus, a possible data interpretation was given based on the FTIR studies below and taking into account the empirical observations on the sols. In curve B the most important features are three peaks at 990 $cm^{-1}$ (a), 960 $cm^{-1}$ (b), and 925 $cm^{-1}$ (c) that can be identified as the Mo−O stretch in the presence of Cl (the Mo═O stretch, reported in the same position, should be excluded since even in the films heated at 250 °C such a bond is still absent), a Mo(V) vibration, and a Mo(IV) vibration, respectively. Curve C shows that upon water addition the Mo(V) peak disappears while bands a and c are broadened. No bands can be ascribed to Mo(VI), and a sharp peak appears at about 800 $cm^{-1}$ (d), together with two weaker bands to the side. This last group of bands is attributed to a Mo−OH vibration, in close analogy with a similar group of bands reported in the FTIR spectra by Mendez-Vivar et al.[7a] These results are interpreted as follows: since in dimers only Mo(V) should be observed, it is likely that actually more complex structures (for instance, linear chains of octahedra formed by methoxo bridges) are present in the unhydrolyzed sol, explaining the presence of Mo(IV). Upon water addition, the Mo−$OCH_3$ and Mo−Cl bonds are hydrolyzed. The hydrolysis of Mo−Cl (decrease of band a) in terminal octahedra would result in the formation of M−OH bonds that give rise to further bridging, resulting in the disappearance of band b as a result of the decrease of terminal Mo(V) species. Bridging of octahedra by OH groups is supposed instead of condensation since no Mo(VI) bands appear. The hindering of condensation reactions explains the sol stability. It in turn may be partly due to steric factors connected with the complex structures in the sol.

**B. Deposition of Thin Films onto Oxidized Silicon**. If the as-hydrolyzed sol is used for depositing thin films onto the oxidized silicon substrate, in general the adhesion of the film is very poor and after drying it is completely withdrawn from the substrate. This problem is common with sols prepared by inorganic precursors, while it is well-known that alkoxide-derived sols allow routine deposition of uniform thin films. There are many possible reasons for this behavior of inorganic sols, which can eventually overlap and depend on the sol processing route: (a) a lower mean number of M−OH bonds may form upon hydrolysis if compared to alkoxide-derived sols; (b) dense colloids formed by precipitation−peptization processes are not highly interpenetrating structures during the film formation and do not have as many condensation sites as "polymeric" sols; (c) the sol may be affected by a high surface tension. In the case of the molybdenum chloroalkoxide, the problem cannot be related to the presence of very dense structures in the sols since, as evidenced before, the processing route does not result in extensively polymerized structures. For this reason CTAB was added to the sol to decrease its surface tension. An actual variation in the surface tension due to the CTAB addition could not be explicitly measured since the sol spread very rapidly, but the change in the film deposition is dramatic: once CTAB is completely dissolved in the sol, the film after the spin-coating process is extremely uniform and completely covers the substrate. CTAB has a very general usefulness, it is easier to eliminate with the heat treatments than other more complex surfactants, and we have successfully applied it to improve the adhesion

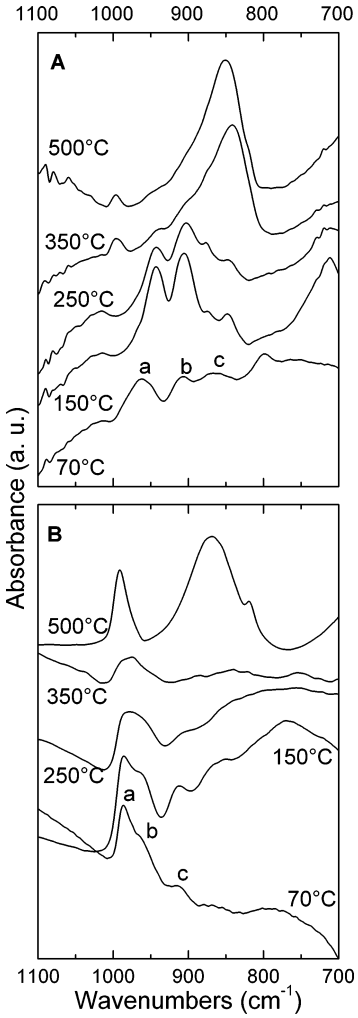


**Figure 3.** FTIR spectra measured on thin films deposited onto silicon (A) and powders (B) heat-treated at the indicated temperatures. The labeled peaks are described in the text.

of thin films of other systems such as $In_2O_3$, $WO_3$, $SnO_2$, and $In_2O_3-SnO_2$. The concentration of CTAB has to be tuned for each system since, beyond a certain threshold, CTAB particles appear on the surface of the dried film that may have a negative impact on the film uniformity and its adhesion, while below the threshold the film adhesion decreases.

**C. Chemical Evolution of Films and Powders with the Heat Treatments**. Upon polymerization, not depending on whether it occurs during the film formation or the sol destabilization or evaporation, the product assumes a typical blue color, indicating the coexistence of different Mo oxidation states, whose relative abundance and the evolution with heating temperature depend on the material typology. This view is suggested by the FTIR spectra, which, together with the analysis of the XPS results, give further insight into the changes of the Mo oxidation state. Part A in Figure 3 shows the FTIR spectra measured on thin films heated at temperatures ranging from 70 to 500 °C. In the film dried at 70 °C three bands at 960 $cm^{-1}$ (a), 910 $cm^{-1}$ (b), and 864 $cm^{-1}$ (c) are attributed to the Mo−O−Mo vibrations of Mo(V), Mo(IV), and Mo(VI), respectively.[8b] This result would seem indicative of a highly dense structure, a result supported by the XPS results concerning the chlorine region (Figure S1 of the Supporting Information). They show that even in the film dried at 70 °C no chlorine can be detected, indicating complete hydrolysis of the Mo−Cl bond. This conclusion is further supported by the corresponding FTIR curve, where a band at 990 $cm^{-1}$ for the Mo−O stretch in the presence of Cl[8b] is completely absent. The extensive hydrolysis of the Mo precursor during the film formation thus favors a highly cross-linked structure already in the dried film. In the case of thin films the XPS data are not helpful in the analysis of the Mo oxidation state, since they indicate that only the Mo(VI) state would be present, which is in contradiction with the FTIR spectra and the blue color of the film heated at 70 °C. This discrepancy is most probably due to extensive oxidation of the thin surface layer probed by the XPS beam. With an increase in the heating temperature no significant changes in the FTIR bands are observed until the film is heated at 350 °C, when the typical spectrum of α-$MoO_3$ appears even if the bands are distorted and shifted and the Mo−O−Mo stretch at 820 $cm^{-1}$ is overlapped with the band at 850 $cm^{-1}$ due to the same vibrations. The behavior of powders is markedly different from that of films. In the FTIR curve measured on the powders heated at 70 °C, shown in part B of Figure 3, an intense peak at 990 $cm^{-1}$ (a) is due to the Mo−O stretch in the presence of chlorine and possibly to the Mo=O stretch.[13] Chlorine is clearly evidenced in the XPS survey shown in part A of Figure 4. This result shows that hydrolysis of the Mo−Cl bond is not complete in the as-obtained powder,

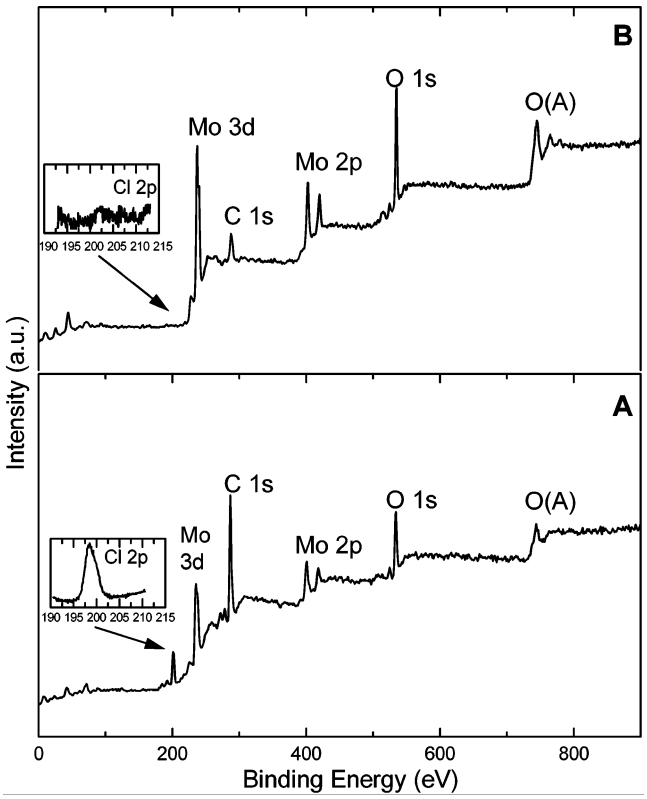


**Figure 4.** XPS survey spectra measured on powders heated at 70 °C (A) and 500 °C (B). The insets show the Cl 2p region for each sample, evidencing the chlorine disappearance in the sample heated at 500 °C.

(13) Seguin, L.; Figlarz, M.; Cavagnat, R.; Lassegues, J.-C. *Spectrochim. Acta, A* **1995**, *51*, 1323.

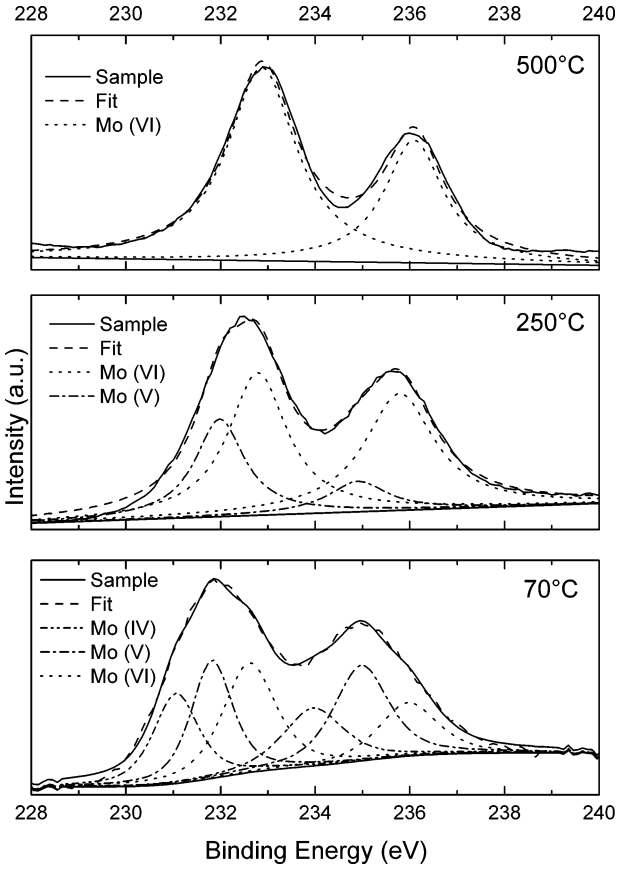


**Figure 5.** XPS experimental spectra and fits of the Mo 3d region for the powders heated at the indicated temperatures.

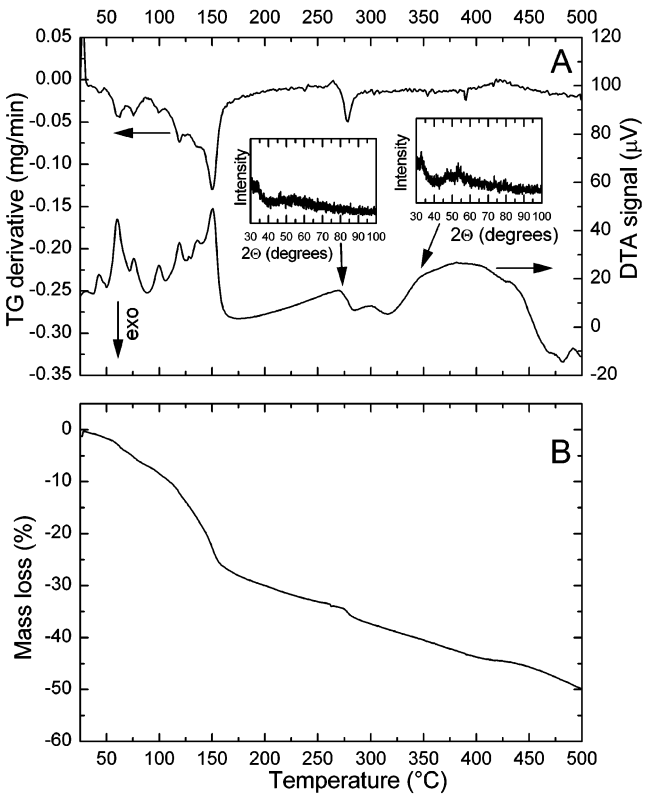


**Figure 6.** DTA trace and TG derivative (A) and TG curve (B) measured on the dried sol. The insets in (A) show the XRD patterns measured on the dried precursor heated at the temperatures indicated by the arrows (see the text).

and indeed, only the bands at 957 $cm^{-1}$ (b) for Mo(V) and at 915 $cm^{-1}$ (c) for Mo(IV) are detected. This situation is partially confirmed by the XPS data for the Mo region shown in Figure 5, where the deconvolution (detailed results for the Mo(X) peak positions are given in Table S1 of the Supporting Information) of the Mo signal displays the presence of a Mo(IV) doublet but also of a broad band resulting from Mo(V) and Mo(VI).

The latter is not seen in the FTIR spectra and could result from surface oxidation. In Figure 4 the intense peak of C 1s can be observed, which strongly decreases after the heat treatment at 500 °C. Since the only source of carbon, apart from the adventitious contamination, is the methoxo ligand, this is a further indication of the incomplete hydrolysis in powders. This result has to be compared with the XPS survey for films in Figure S1 (Supporting Information), showing, already heating at 70 °C, a reverse ratio between the intensity of the Mo and the C peaks if compared with the powders. This observation indirectly confirms the different hydrolysis behavior in thin films and powders. With an increase of the heating temperature up to 250 °C, chlorine is eliminated (Figure S2, Supporting Information), and the survey for the powder heated at 500 °C in part B of Figure 4 confirms that even this sample is chlorine free. Thus, the broad peak at 990 $cm^{-1}$ in the FTIR curve for the sample heated at 250 °C is due to an envelope of the Mo=O stretch at 990 $cm^{-1}$ and the Mo(V) vibration at 957 $cm^{-1}$. The XPS analysis in Figure 5 for the 250 °C sample confirms the presence of Mo(VI) and Mo(V) and the disappearance of Mo(IV). After heating at 350 °C, the 957 $cm^{-1}$ FTIR band strongly decreases, and finally after heating at 500 °C, the typical spectrum of α-$MoO_3$ appears, which is practically identical to that shown by Seguin et al.[13] and is closely related to the corresponding XPS curve in Figure 5, only showing the Mo(VI) component. Thus, the powders are not completely hydrolyzed after drying at 70 °C and undergo a structural rearrangement through heating, during which the oxidation state of Mo progressively increases up to VI due to the ongoing hydrolysis and condensation reactions and the consequent formation of the final structure.

A possible reason for this difference between films and powders is the compaction of the powder precursor during the evaporation process, making chlorine more difficult to evaporate. It is interesting to observe that these results are closely related with those obtained by Dong and Dunn in ref 8b. In that work the authors used $CH_3CN$ to complex the Mo precursor to prevent the formation of Mo=O terminal bonds, which would hinder the formation of three-dimensional gels. In this work we have obtained 3D continuous gels in the case of films, where the Mo=O is completely absent until heat treatment at 350 °C, while from sol evaporation no monolithic gels could be obtained, and in that case the Mo=O is clearly visible already in the dried sol (see the spectra above).

A dynamic representation of the phenomena occurring during heating is given by the thermal analysis on the precursor powder, shown in Figure 6. Part A of the figure shows the DTA trace together with the derivative of TG, whose curve is shown in the lower part of the figure. The correspondence between the peaks in the TG

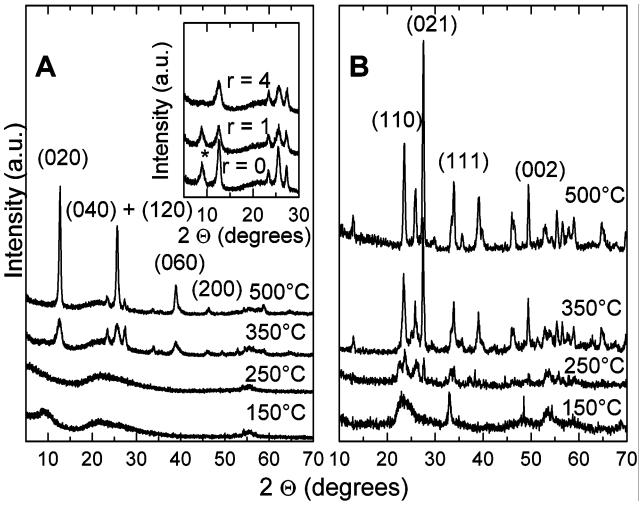


**Figure 7.** XRD patterns measured on thin films deposited on silicon from a sol with $r = 4$ (A) and on the precursor powders (B) heat-treated at the indicated temperatures. The asterisk in the inset indicates the hexagonal phase of $MoO_3$ in thin films prepared with the indicated values of $r$ and heat-treated at 350 °C.

derivative and in the DTA trace helps in determining the phenomena that result in mass variation of the sample. The DTA trace can be divided into different regions. In the temperature range up to about 150 °C different endothermic phenomena take place, each resulting in a mass loss, that can be identified, in agreement with the previously described results, as the loss of water and methanol, both desorbed and resulting from hydrolysis and condensation reactions, and as the chlorine elimination. Most of the mass loss occurs in this region, but it continues throughout the heating, showing that the elimination of residuals affects the whole process. An exothermic peak at 280 °C accompanied by a mass loss is attributed to the oxidation of organic residuals. The evolution of the $CH_2$ and $CH_3$ stretching bands in the high-frequency part of the FTIR curves, related to the methoxo ligand and shown in Figure S3 of the Supporting Information, closely follows the present interpretation of the DTA. Another exothermic peak at about 350 °C, not accompanied by a mass loss, was attributed to the crystallization of $MoO_3$. For confirming this interpretation, XRD patterns were acquired on powders heated at temperatures just before and after the peak, and suddenly carried out of the oven as soon as the temperature was reached, to reproduce as much as possible the conditions of the thermal analysis. The results, shown in the insets, confirm that this peak can be attributed to crystallization. Finally, a weak exothermic peak is observed at about 480 °C with a slight mass gain, due to final oxidation of the sample.

**D. Structure and Morphology of Films and Powders with the Heat Treatments**. Part A of Figure 7 shows the XRD patterns of $MoO_3$ films with $r = 4$, annealed at different temperatures. The samples treated at lower temperatures, 150 and 250 °C, do not present any crystallographic evidence of crystalline $MoO_3$ phases or similar. As the annealing temperature increases up to 350 °C, peaks of orthorhombic α-$MoO_3$ phase (JPCDS 5-508) appear. The small peak at approximately $2\vartheta = 9°$ has been attributed to the (100) reflection of the $MoO_3$ hexagonal phase (JPCDS 21-569), thus indicating the presence of a mixture of hexagonal and orthorhombic phases. At 500 °C the mixed oxide transforms into an orthorhombic α-$MoO_3$ structure with a preferential orientation along the [010] direction. As shown in the figure, an amorphous component is still present at 350 and 500 °C. The least-squares refinement of the unit cell parameters for the orthorhombic phase leads to $a = 3.948 \pm 0.011$ Å, $b = 13.909 \pm 0.018$ Å, and $c = 3.688 \pm 0.011$ Å and $a = 3.963 \pm 0.002$ Å, $b = 13.897 \pm 0.008$ Å, and $c = 3.701 \pm 0.005$ Å for the films treated at 350 and 500 °C, respectively. A similar behavior was found in $MoO_3$ films with $r = 0$ and $r = 1$, which show the development of a mixture of hexagonal and orthorhombic crystalline phases with an increase of the heating temperature up to 350 °C, and only the orthorhombic one, with a strong [010] texture, at 500 °C. The main difference, with respect to the samples with $r = 4$, is the larger amount of hexagonal phase, as reported in the inset in part A of Figure 7, where the X-ray patterns of films treated at 350 °C and with different $r$ values are shown. A Rietveld quantitative analysis[14] lead to hexagonal phase amounts of about 12% and 20% for films with $r = 1$ and $r = 0$, respectively. In the films with $r = 4$ the hexagonal phase content is much smaller, as the peak can be barely seen, and we can affirm that its amount is close to 3−5%, which is the detection limit of the diffraction technique. Then, the content of hexagonal phase seems to be influenced by the different $H_2O$:Mo molar ratios. Our results are in agreement with data reported in the literature: the structural transformation from hexagonal to stable orthorhombic α-$MoO_3$ has been observed around 350 °C,[15] and it occurs in such a way that the resulting α-phase displays a strong [010] preferred orientation.[16] The crystallite size, for the films with $r = 4$, was calculated from the width of the reflections (020), (040), and (060), and it increased from $73 \pm 5$ to $149 \pm 3$ Å when the annealing temperature was increased from 350 to 500 °C, respectively. The thermal treatment favors an increase in the coherently scattered area, with narrow peaks and a better crystalline quality of the films. The evolution of the XRD patterns closely follows the evolution of the typical α-$MoO_3$ vibrations observed in the FTIR curves in Figure 3. The XRD patterns measured on powders and displayed in part B of Figure 7 show that the sample heated to 250 °C is poorly crystallized, while the structure of α-$MoO_3$ appears after heating at 350 °C, even though the peaks are slightly distorted. After heating at 500 °C, the crystallization of α-$MoO_3$ appears complete.

No evidence of the hexagonal phase was obtained for a powder prepared with $r = 0$ and heated at 350 °C. The XRD patterns on powders follow the evolution of the FTIR spectra but less clearly in the case of the 350 °C heated sample, which appears extensively crystallized even though the FTIR curve does not show as clear a structure as that of the sample heated at 500 °C (see

(14) Bish, D. L., Post, J. E., Eds. *Modern Powder Diffraction*; Reviews in Mineralogy; The Mineralogical Society of America: Washington, DC, 1989; Vol. 20.
(15) Muraoka, Y.; Grenier J. C.; Petit, S.; Pouchard, M. *Solid State Sci.* **1999**, *1*, 133.
(16) Julien, C.; Khelfa, A.; Hussain, O. M.; Nazri, G. A. *J. Cryst. Growth* **1995**, *156*, 235.

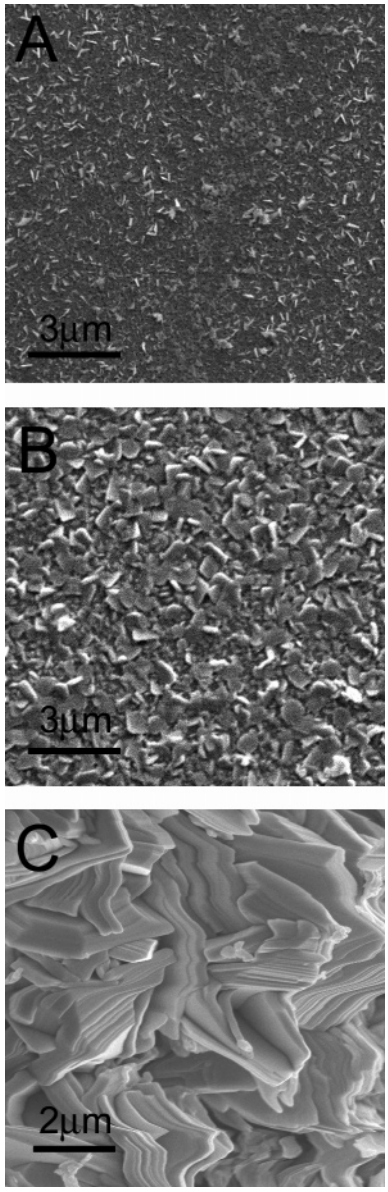


**Figure 8.** SEM morphology of $MoO_3$ thin films deposited on silicon and heat-treated at 350 °C (A) and 500 °C (B) and of a powder heat-treated at 500 °C (C).

Figure 3). Figure 8 shows the morphology of the films heated at 350 °C (A) and 500 °C (B) and of the powders obtained after heat treatment of the precursor at 500 °C. The film heated at 350 °C is characterized by a rough morphology where small, elongated particles are dispersed on the surface. After heating at 500 °C, larger particles appear in the form of flat platelets with a size of about 1 $\mu$m, explaining the opacity of the film as seen by the naked eye. This morphology can be correlated with that of the powders heated at 500 °C (C), where a lamellar structure is observed, in agreement with the known structure of α-$MoO_3$. Thus, the platelets observed in the film heated at 500 °C are most probably the result of the layered structure and of the larger size of the crystalline domains if compared with the film heated at 350 °C (see above). In conclusion, the molybdenum chloromethoxide has been shown to be a convenient and easily processable precursor for the preparation of α-$MoO_3$ thin films and powders. Uniform thin films on oxidized silicon can be deposited by adding a surfactant to the sol, improving the wetting of the substrate. The chemical and structural evolution of the powders with the thermal treatment is different from that of thin films and is influenced by the presence of unhydrolyzed Mo−Cl bonds in the precursor. The powders are chlorine free after the heat treatment at 250 °C.

**Acknowledgment.** We thank Enrico Melissano for the SEM observations, Donato Cannoletta for the XRD measurements on the powders, Paolo Rotolo for the XPS measurements, and Giuseppe Ciccarella for the assistance with the FTIR measurements. M.E. acknowledges the financial support from the National Council of Research (CNR) for a short-term stay at the University of Barcelona (Spain), and Raul Diaz, Tariq Jahwari, and Prof. Joan. R. Morante at the University of Barcelona for the Raman spectra, the many helpful discussions, and the friendly environment. This work was partially supported in the context of the GASMOH (Grant ICA2-CT-2000-10041) project.

**Supporting Information Available:** XPS survey scan for a film heat-treated at 70 °C, evolution of the Cl 2p XPS signal for powders heat-treated at different temperatures, and evolution of the high-frequency part of the FTIR spectra measured on powders heat-treated at different temperatures (PDF). This material is available free of charge via the Internet at http://pubs.acs.org.

CM048997I